MOLECULAR PHYSICS, 1986, VOL. 58, NO. 4, 763–788

A Monte Carlo investigation of the Lebwohl–Lasher lattice model in the vicinity of its orientational phase transition

by U. FABBRI
CINECA, Via Magnanelli, 40033, Casalecchio, Bologna, Italy
and C. ZANNONI
Istituto di Chimica Fisica, Universitá, Viale Risorgimento, 4, 40136 Bologna, Italy

(*Received 6 January 1986; accepted 5 February 1986*)

The Lebwohl–Lasher model of nematogens consists of a system of particles placed at the sites of a cubic lattice and interacting with a pair potential $U_{i,j} = -\varepsilon_{ij} P_2(\cos \beta_{ij})$, where ε_{ij} is a positive constant, ε, for nearest neighbours particles i and j and β_{ij} is the angle between the axis of these two molecules. We have investigated this model using Monte Carlo simulations with periodic boundary conditions on a $30 \times 30 \times 30$ lattice while the largest system previously studied was $20 \times 20 \times 20$. The number of simulation runs near the transition is also significantly higher than in previous simulations to allow a more precise determination of the orientational transition temperature T^*_{NI}. The transition temperature has been placed at $kT/\varepsilon = 1{\cdot}1232 \pm 0{\cdot}0006$, refining previous estimates. Orientational order parameters $\langle P_2 \rangle$, $\langle P_4 \rangle$ have been calculated and a new algorithm is proposed for the computation of $\langle P_4 \rangle$. Particular attention has been devoted to pretransitional properties. Pair correlations $G_2(r)$, $G_4(r)$ as well as the second rank g_2-factor are reported. g_2 is found to diverge at a temperature $T^*_{NI^*} = kT/\varepsilon = 1{\cdot}1201 \pm 0{\cdot}0006$ and to fit the Landau–de Gennes behaviour except near the transition. Our results indicate therefore that the Lebwohl–Lasher model can yield the small difference between the nematic–isotropic transition temperature and the isotropic phase limiting instability temperature without the need of introducing additional terms in the potential.

1. INTRODUCTION

In the Lebwohl–Lasher (LL) model [1–11], a system of uniaxial particles placed at the sites of a cubic lattice interacts through a nearest neighbour pair potential of the form

$$U_{i,j} = -\varepsilon_{ij} P_2(\cos \beta_{ij}), \tag{1}$$

where ε_{ij} is a positive constant, ε, for nearest neighbours particles i and j, $P_2(x)$ is a second Legendre polynomial and β_{ij} is the angle between the axis of these two molecules. From a formal point of view (1) is a simplified version of the attractive anisotropic interaction put forward by Maier and Saupe [9] and is sometimes referred to as Maier–Saupe model. The Lebwohl–Lasher (LL) model has become

a prototype for computer simulations [1–8] and theoretical calculations [9–17] on systems which undergo a nematic–isotropic like orientational phase transition. In this sense its role is somewhat similar to that covered by the Ising and Heisenberg models in the field of magnetic phase transitions [18–21]. However, the number of computer simulations and rigorous studies on the LL model is still a minute fraction of what is available for magnetic systems. The computer simulations have been performed using the Monte Carlo method on systems of various size, from $10 \times 10 \times 10$ [4] to $20 \times 20 \times 20$ [1, 3, 7] and the molecular dynamic method on a $10 \times 10 \times 10$ lattice [5]. A larger size system of $50 \times 50 \times 50$ has been studied [2], but only with an approximate technique and with a quantization of the orientations permissible to a molecule to just 128. The $20 \times 20 \times 20$ LL lattice mentioned above has been studied by three different groups [1, 3, 7]. The system has been found to give a phase transition with a weak first order character. The nematic–isotropic transition temperatures T^*_{NI} reported from these studies are 1·124 [1], 1·119 [3], 1·127 [7] in dimensionless units $T^* = kT/\varepsilon$. It is somewhat paradoxical that computer simulations on such a well defined system should give uncertainties of the order of 0·5 per cent in T^*_{NI}. This uncertainty, seemingly small at first sight, would correspond to something of the order of 1·5 to 3 K in a real life experiment on a typical room temperature nematic. Thus it seems that computer calorimetry cannot offer the kind of resolution obtained experimentally which is of the order of 10^{-2} K in routine high resolution measurements and below 10^{-3} K for studies of phase transitions and pretransitional properties [22]. The situation is also very different from that of Ising spin lattices, where arrays up to $1080 \times 1080 \times 1080$ have been studied [18]. This is due not only to the long history and importance of the Ising model, but also to the fact that it is obviously much easier to study a system of spins with just two possible orientations. In particular the fact that the state of an Ising spin can be represented with just one bit has encouraged the use of special data structures and multispin coding techniques [18] which are unfortunately not suitable for the study of continuous variables. In any case it seems that larger systems, better boundary conditions [5] etc. need to be used if the nematic–isotropic transition and its critical exponents are to be studied in detail. The purpose of the present work is to report results of a series of Monte Carlo experiments on $30 \times 30 \times 30$ lattices in a temperature region close to the transition. We shall concentrate in particular in getting a better estimate of the transition temperature and of the other relevant observables near the transition. We shall also be interested in studying pretransitional behaviour of order parameters and pair correlations [6, 23–24]. This is necessary if we are to ascertain whether the LL model contains the basic ingredients to describe the subtleties of the nematic–isotropic transition. One particularly striking point is the experimental observation that the difference D^* between the nematic–isotropic transition temperature and the temperature $T^*_{NI^*}$ where the isotropic phase becomes absolutely unstable is very small, i.e. about 1 K [24–25]. Despite numerous attempts, present theories have been unable to quantitatively explain this observation. A Molecular Field treatment [14] gives a value thirty times bigger than the observed one. This poor estimate is improved, but not sufficiently, by two-, three- and four-site cluster extensions [15]. Renormalization group techniques [17] also seem to fail to provide the small experimental D^*. It has been suggested that this is due to a fundamental insufficiency in the LL model and that in order to explain the observed D^* one should consider additional

biaxial terms in the potential [26]. It is important to see if a simulation study of the LL model, which yields essentially exact results, is able to produce the fundamental quantity D^*. Here we shall offer some evidence that this is the case for our simulation.

2. The simulation

All the calculations reported in this paper have been performed on a $30 \times 30 \times 30$ cubic lattice system with periodic boundary conditions. The particles are assumed to interact through the nearest neighbour LL potential in equation (1). The standard Metropolis Monte Carlo algorithm [4, 18–19] has been used to generate equilibrium configurations. The simulation at the first temperature studied ($T^* = 1{\cdot}00$) was started from a completely aligned system. The simulations at the other temperatures have been run in sequence starting from an equilibrium configuration at a nearby lower temperature. The orientation of each particle is stored as cos β and α, where β and α are the polar and azimuthal angles of the symmetry axis of each particle. The configuration of the system is given by the set of N such orientations $\{\alpha_i, \beta_i\}$ where N is the number of particles. We move one particle at a time and we shall call a cycle a set of N attempted moves. A new configuration is generated by choosing a particle at random out of those that we have not yet attempted to move during the current cycle [27]. To this end a simple random shuffling algorithm is used [28]. This procedure ensures that every particle gets an equal chance of moving at every cycle, while removing the unnecessary regularities in particle selection. The orientation of the chosen particle is then changed by generating a new random value of the variable cos β and α. We are close enough to the transition temperature to get a satisfactory rejection ratio even with these possibly large orientational jumps. In every simulation a minimum of 3000 cycles are used for equilibration and thus rejected when calculating averages. Near the transition, i.e. from $T^* = 1{\cdot}123$ to $T^* = 1{\cdot}124$ at least 10 000 cycles are rejected and runs up to 70 000 cycles follow. Equilibration is checked by monitoring fluctuations in the observables; plots of these quantities versus the number of cycles are not reported for reasons of spaces but are available from the authors. The simulations are divided in M trajectory segments of 1000 cycles each. Errors in the observables at a certain temperature are evaluated from the standard deviation from the average in these M computer experiments.

The running of large scale Monte Carlo simulations requires generating a considerable number of random variables. For our systems we need many millions of random numbers at each temperature. These are produced using the RANF routine available on the CRAY with some precautions briefly discussed in what follows. In linear congruential algorithms like that adopted in the RANF routines [29] a new pseudo-random number x_{n+1} is generated by the previous one through the simple relation [28]

$$x_{n+1} = ax_n \bmod 2^p \tag{2}$$

where a is a suitable multiplier and the recurrence is started from a proper seeding [29]. This procedure may cause various problems. The method will intrinsically lead to the same sequence after a maximum cycle length of 2^p, where p is the number of bits available. In the CRAY X-MP/12 used here we have a 48 bit integer mantissa (as in the CDC 176) so $p = 48$. The size periodicity is there-

fore not our main problem on this machine. Problems with generators like equation (2) are relatively more severe when the random numbers are employed in pairs or triplets to determine the particles orientation [28]. This same generator has in particular caused problems when applied with vectorized algorithms to large Ising lattices whose linear size is a large power of 2 [30]. In [30] $128 \times 128 \times 128$ spins were treated and large groups of random numbers chosen together and employed sequentially. We have decided to reduce the risk of short range correlations between random numbers by using the algorithm of Bays and Durham as described in Knuth's book [28]. In essence we proceed by filling an array of size 1024 with random numbers produced with the RANF generator. Then another random number y_i is generated with RANF. This is used, taking its value modulo the array length, to pick up the next number which is actually going to be used from the array. This number is then replaced by y_i itself in the array. This scrambling is expected to produce a "considerably more random sequence" than the original one [28].

3. Observables and their calculation

3.1. *Generalities*

Every observable of interest A is sampled at every cycle. After a certain number of cycles (here 1000) an average is calculated thus coarse graining the trajectory. A further grand average over M such segments is then calculated

$$\langle A \rangle = (1/M) \sum_J A^J \tag{3}$$

together with the attendant standard deviation σ_A. We have also calculated histograms of the frequency of occurrence of a certain value A^J during the simulation by sorting the M observed samplings in a suitable number of buckets. As we shall see this will be especially useful in order to investigate the neighbourhood of the transition.

Energy The energy for the lattice system with periodic boundary conditions is

$$U_N = -(1/2) \sum_{i=1}^{N} \sum_{j=1}^{N} \varepsilon_{ij} P_2(\cos \beta_{ij}); \qquad \text{with } i \neq j \tag{4a}$$

$$= -(Nz\varepsilon\sigma_2)/2, \tag{4b}$$

where $z = 6$ is the coordination number and $\sigma_2 = \langle P_2(\cos \beta_{12}) \rangle$ is a short range order parameter averaged over neighbour particles.

The results of the simulation for the dimensionless single particle energy $U^* = \langle U \rangle / N\varepsilon$ at the various reduced temperatures $T^* = kT/\varepsilon$ studied are shown in figure 1. We see clearly that a sharp change of slope occurs suggesting the onset of a first order transition. We have also calculated histograms of the frequency of occurrence of a certain value of the energy $P(U^*)$. In general the histograms consist of extremely narrow peaks, but their behaviour becomes particularly interesting near the transition. Since it is difficult to present graphical data for all the histograms, we have chosen, for the sake of brevity, to tabulate some of their most important statistical parameters. We have calculated the first four cumulants of $P(U^*)$ and obtained the results reported in table 1. We remember that the cumulants k_n [31] of a distribution $f(x)$ are related to the moments of

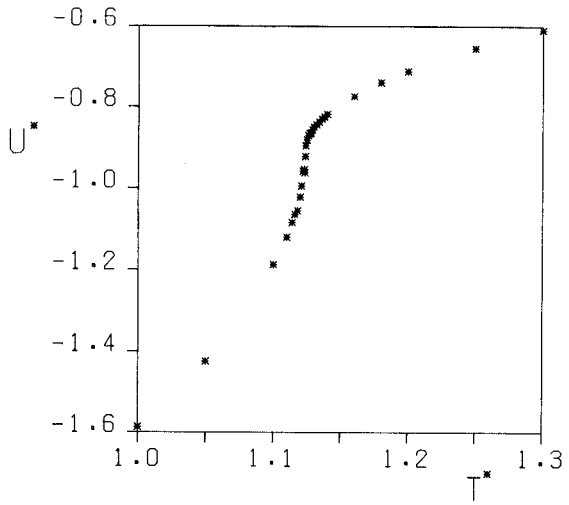

Figure 1. The single particle energy $U^* = \langle U \rangle / N\varepsilon$ vs dimensionless temperature $T^* = kT/\varepsilon$ for the Monte Carlo simulation of the 30 × 30 × 30 Lebwohl–Lasher model.

Table 1. The first four cumulants, k_1, k_2, k_3, k_4 of the distribution $P(U^*)$ of the energy values observed during the simulations.

T^*	k_1	$k_2 \times 10^3$	$k_3 \times 10^5$	$k_4 \times 10^6$
1·1140	−1·0851	0·552	0·182	0·006
1·1160	−1·0650	0·447	0·092	−0·032
1·1180	−1·0562	0·370	0·211	−0·039
1·1200	−1·0225	0·460	−0·025	−0·039
1·1210	−0·9939	0·797	−0·183	−0·119
1·1220	−0·9614	1·991	2·327	−3·992
1·1230	−0·9558	1·258	1·998	−0·284
1·1235	−0·9626	1·500	1·960	−0·997
1·1238	−0·9249	1·425	−2·506	−1·287
1·1240	−0·8959	0·917	−3·085	1·276
1·1250	−0·8817	0·367	−0·181	−0·015
1·1260	−0·8709	0·264	−0·106	0·000
1·1270	−0·8656	0·185	−0·032	−0·005
1·1280	−0·8651	0·317	−0·451	0·103
1·1290	−0·8563	0·205	−0·056	0·010
1·1300	−0·8503	0·135	0·037	0·004
1·1320	−0·8450	0·138	−0·020	−0·005
1·1340	−0·8382	0·152	−0·019	0·006
1·1360	−0·8309	0·130	0·007	−0·004
1·1380	−0·8261	0·131	−0·041	0·001
1·1400	−0·8192	0·123	−0·026	0·004
1·1600	−0·7752	0·086	0·002	0·001
1·1800	−0·7406	0·073	−0·006	0·000
1·2000	−0·7122	0·068	0·001	0·000
1·2500	−0·6547	0·053	−0·002	0·000
1·3000	−0·6095	0·046	−0·001	0·000

the distribution. In particular for the first four cumulants of interest here we have for the generic variate x

$$k_1 = \langle x \rangle, \tag{5a}$$

$$k_2 = m_2, \tag{5b}$$

$$k_3 = m_3, \tag{5c}$$

$$k_4 = m_4 - 3m_3^2, \tag{5d}$$

where m_n is the nth central moment

$$m_n = \sum_b (x_b - \langle x \rangle)^n p_b, \tag{6}$$

and p_b is the population of the histogram at bucket b. We recall that for a gaussian the first cumulant gives the centre and the second the width, while cumulants above the second are zero. Inspection of table 1 shows that k_2, i.e. the width of the peaks near the transition becomes about twenty times larger than that of the peaks in the isotropic phase. In the same region the third cumulant significantly differs from zero and changes sign, going from positive below the transition to negative. The fourth cumulant illustrates the gaussian character of the peaks as soon as one moves from the transition. In figure 2 we report some of these

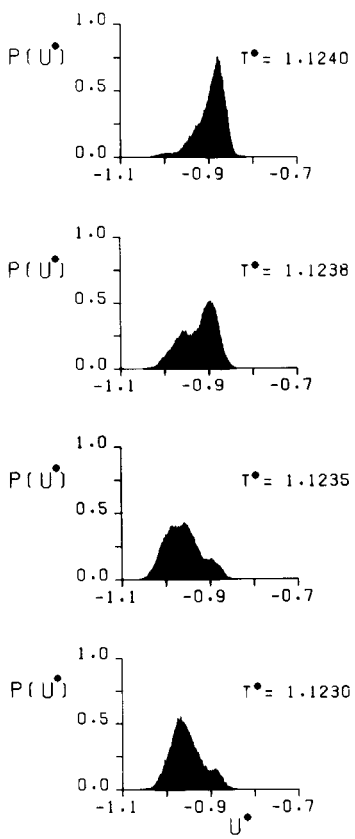

Figure 2. Histograms of the distribution of energy values obtained during the simulation for four temperatures T^* in the transition region.

histograms in the transition region (1·121 to 1·124). Here we do not just observe an overall shift, but rather we see indications of the double peak behaviour expected for a first order phase transition [1]. The intensity of the two peaks changes with temperature showing that the transition is situated in this relatively narrow range.

3.2. *Heat capacity*

The heat capacity of the system C_V^* has been evaluated by differentiating U^* with respect to T^*. This is done by first fitting a smoothing cubic spline to the data points (ICSSCV from IMSL [32]) then taking the derivative. We have not broken the temperature interval in two regions and fitted separately, since this would somehow amount to assuming beforehand a true first order phase transition. We know from magnetic system studies [18–21, 33] that our system will mimic the occurrence of such a phase change by exhibiting a sharp change in the slope of the energy vs. temperature curve. These results are shown in figure 3 as the continuous curve and the values of C_V^* at the experimental temperatures are reported in the general summary table in the Appendix. Errors in C_V^* reported in the Appendix have been estimated by the uncertainty in the energy repeating the differentiation procedure. We identify the orientational transition temperature with the position of the heat capacity maximum and find the value $T_{NI}^* = 1{\cdot}1232 \pm 0{\cdot}0006$.

Based on this value for the transition temperature and on the previously given energy histograms, we estimate the entropy change as

$$(S_N - S_{iso})/R = (U_N^* - U_{iso}^*)/T_{NI}^* \leqslant 0{\cdot}05. \tag{7}$$

We also notice that the heat capacity peak is asymmetric and much steeper on the hot side of the transition. The temperature resolution of our data is really not

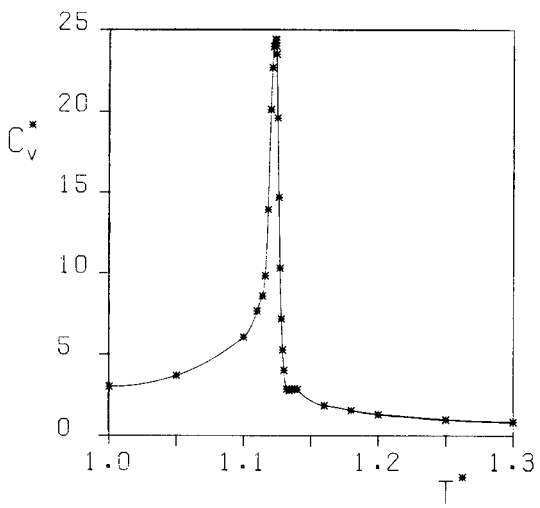

Figure 3. The heat capacity C_V^* obtained from differentiation of energy vs T^* as described in the text (continuous curve). Values corresponding to the actual simulation temperatures T^* are also shown as the symbols.

sufficient to get very precise estimates of the exponents. However, it seems interesting to obtain some approximate estimates. An estimate of the heat capacity exponents has been obtained by a non-linear least square fit of C_V^* to the following expression [18, 33]

$$C_V^* = A \Big/ \left[\frac{T^*}{T_{NI}^*} - 1 \right]^{\alpha} + B.$$

We use data for T^* above 1·124 to limit the rounding due to the finite sample size and to the numerical differentiation through splines and assume T_{NI}^* as previously determined. We find that our data can be fitted using $A = 0{\cdot}363$, $B = -1{\cdot}44$, $\alpha = 0{\cdot}596$. We recall that experimentally values of α very close to 0·5 have been found [22]. Fits on the cold side of the transition are not reported because of the small number of data points available.

3.3. *Second and fourth rank order parameters*

The determination of orientational order parameters is an important part of a model liquid crystal simulation, albeit by no means a trivial one [4]. The major difficulty stems from the overall rotational symmetry existing in the system [34] in the absence of external fields and when using periodic boundary conditions [8]. This symmetry somewhat conflicts with the possibility of defining order parameters $\langle P_L \rangle$ for a molecule with respect to a uniform director, i.e. as

$$\langle P_L \rangle = \int_0^1 d\cos\beta \; P_L(\cos\beta) \; P(\cos\beta) \Big/ \int_0^1 d\cos\beta \; P(\cos\beta), \tag{8}$$

for L even, where β is the orientation of the particle axis with respect to the director and $P(\cos\beta)$ is the singlet orientational distribution. During the simulation the director may fluctuate from one configuration to the next and thus the order parameter is normally calculated with respect to the instantaneous preferred direction. Here we briefly summarize the evaluation of this second rank order parameter $\langle P_2 \rangle_\lambda$ to prepare the ground for introducing an algorithm for the computation of the fourth rank order parameter.

The determination of order parameters in the simulation can be viewed as an idealized experiment. We consider a single molecule property $\mathbf{A} = \mathbf{q} \times \mathbf{q}$, with $\mathbf{q} = (001)$ being a vector directed along the z molecular axis. As an example the properties $\mathbf{A}$, $\mathbf{q}$ could be thought of as a transition tensor and respectively a transition moment in a certain fluorescence depolarization experiment [35]. The average $\langle \ldots \rangle_S$ over the N sample particles of $\mathbf{A}$ will be

$$\langle A_{ab}^L \rangle_S = \frac{1}{N} \sum_{i=1}^{N} \left[\sum_{a',b'} R_{a,a'} \, A_{a',b'}^M \tilde{R}_{b',b} \right]_i, \tag{9a}$$

$$= \langle R_{a,z} \, R_{b,z} \rangle_S, \tag{9b}$$

in the laboratory frame used to define orientations during the simulation.

Here $\mathbf{R}$ is the orthogonal matrix rotating from the laboratory to the molecule frame and we have taken advantage of the fact that $A_{i,j}^M = \delta_{i,z}\delta_{j,z}$. Diagonalization of the matrix $\langle \mathbf{A}^L \rangle_S$ locates the sample director frame (D). We shall take the instantaneous director to be parallel to the direction Z, defined by the eigenvector associated with the largest eigenvalue of $\mathbf{A}$. We can now obtain the second

rank order parameter since

$$\langle A^{D}_{ZZ}\rangle_S = \sum_{a,b} U_{aZ}\, U_{bZ} \langle A^{L}_{ab}\rangle_S, \tag{10a}$$

$$= \langle \cos^2 \beta\rangle_S, \tag{10b}$$

$$= (2\langle P_2\rangle_S + 1)/3, \tag{10c}$$

where $\mathbf{U}$ is the matrix rotating the laboratory into the director frame (i.e. the matrix of eigenvectors of $\langle \mathbf{A}^L\rangle_S$) and the angle β gives the orientation of the molecule axis in the director frame. This procedure corresponds to the well known method for determining $\langle P_2\rangle$ with respect to the instantaneous director from a simulation in a nematic-like phase [4, 34, 36]. There are problems above the isotropic phase transition where the director is loosely defined [8, 36] but no particular problem arises in the ordered phase. In practice the $\langle \mathbf{A}^L\rangle_S$ matrix is calculated and diagonalized at every cycle and its largest eigenvalue is used to give the order parameter for the system with respect to the instantaneous director. This is then averaged (cf. equation 3) to produce the values $\langle P_2\rangle_\lambda$ denoted by asterisks in figure 4. The curve looks fairly continuous although very rapidly changing in the transition region. The derivative of $\langle P_2\rangle_\lambda$ vs. temperature presents in fact a very sharp negative peak with a minimum of about -40 at $T^* = 1{\cdot}1237$. If we take this as the long range order indicator of where the transition occurs, we see that it agrees very well with the short range order indicator provided by the heat capacity. To examine more closely the behaviour of the order parameter it is useful to look at histograms of the frequency of occurrence of a certain $\langle P_2\rangle$ during the simulation. As we did for the energy we shall first condense a description of all these histograms in terms of cumulants (see table 2). Inspection of the cumulants in table 2 shows that the peaks are essentially gaussian except in the region from $T^* = 1{\cdot}1220$ to $1{\cdot}125$. In this range

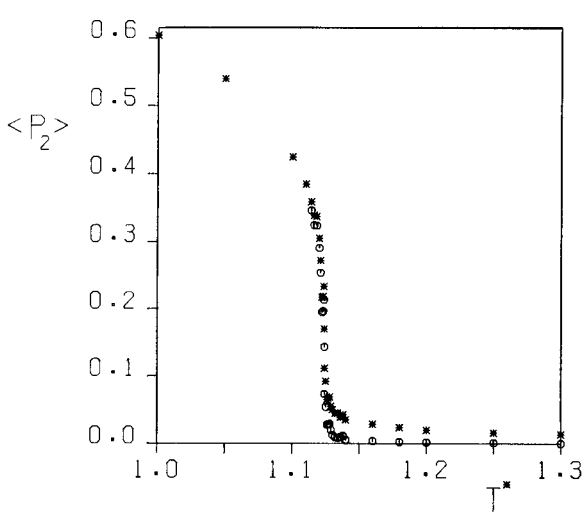

Figure 4. The second rank order parameter $\langle P_2\rangle$ at temperatures T^* as obtained through the diagonalization procedure described in the text. We report the order parameter evaluated from the largest eigenvalue (stars) and from the intermediate one [36] (open circles).

Table 2. The first four cumulants, k_1, k_2, k_3, k_4 of the distribution $P(\langle P_2\rangle_\lambda)$ of the second rank order parameter values observed during the Monte Carlo simulations at temperatures T^*.

T^*	k_1	$k_2 \times 10^3$	$k_3 \times 10^5$	$k_4 \times 10^6$
1·1140	0·3585	0·386	0·00	0·02
1·1160	0·3384	0·417	−0·15	−0·04
1·1180	0·3370	0·267	−0·15	−0·03
1·1200	0·3051	0·467	−0·32	−0·03
1·1210	0·2694	1·305	−1·83	−0·19
1·1220	0·2223	4·977	−19·99	−21·68
1·1230	0·2211	3·214	−20·59	7·39
1·1235	0·2337	3·448	−18·81	5·37
1·1238	0·1746	4·216	1·86	−16·16
1·1240	0·1102	3·783	21·46	−1·85
1·1250	0·0918	1·332	1·00	−0·59
1·1260	0·0647	0·689	0·62	−0·30
1·1270	0·0670	0·590	0·84	−0·01
1·1280	0·0688	1·294	6·31	2·17
1·1290	0·0550	0·683	1·43	0·06
1·1300	0·0497	0·260	0·14	0·00
1·1320	0·0445	0·400	0·95	0·24
1·1340	0·0451	0·318	0·26	0·01
1·1360	0·0384	0·203	0·19	0·03
1·1380	0·0423	0·302	0·46	0·07
1·1400	0·0348	0·151	0·06	0·00
1·1600	0·0284	0·114	0·07	0·00
1·1800	0·0234	0·083	0·05	0·00
1·2000	0·0193	0·049	0·02	0·00
1·2500	0·0153	0·037	0·01	0·00
1·3000	0·0132	0·023	0·01	0·00

the third cumulant and thus the skewness [31] of the distribution change sign reflecting the change in the type of order parameter from a nematic-like to an isotropic like. To illustrate this point we show in figure 5 four histograms of $\langle P_2\rangle$ in the transition region. The distribution of $\langle P_2\rangle$ which is used to give the points in figure 4 changes quite abruptly across the transition, in accord with its expected first order character. Notice that $\langle P_2\rangle_\lambda$ does not go quite to zero above the transition, but rather to a value of the order of $N^{-1/2}$. Eppenga and Frenkel [36] have suggested that a better estimate of the order parameter in the isotropic phase can be obtained by looking at the intermediate, rather than the largest eigenvalue of the matrix $\langle \mathbf{A}^L\rangle_S$ as defined in (9). We have argued elsewhere [8] that the root of the problem is conceptual more than numerical and is connected with the absence of a bona-fide director above the orientational transition. In any case in figure 4 we also show as the empty circles the values of this new order parameter, called here $\langle P_2\rangle_{\lambda_2}$, near and above the transition and we see that they do approach zero more closely than $\langle P_2\rangle_\lambda$. Histograms for this order parameter have also been recorded. The behaviour of the $P(\langle P_2\rangle_{\lambda_2})$ histograms is essentially the same as those of $\langle P_2\rangle_\lambda$ so we shall only report their statistical parameters in table 3. We notice that above the transition the skewness of the distribution of the order parameter calculated according to Eppenga and Frenkel is smaller than that of the $P(\langle P_2\rangle_\lambda)$ distribution. This is of course to be expected since $\langle P_2\rangle_{\lambda_2}$ can fluctuate around zero, while $\langle P_2\rangle_\lambda$ is always non negative. From the histograms

Table 3. The first four cumulants, k_1, k_2, k_3, k_4 of the distribution $P(\langle P_2\rangle_{\lambda_2})$ of the intermediate eigenvalue [36] second rank order parameters observed at various temperatures T^*.

T^*	k_1	$k_2 \times 10^3$	$k_3 \times 10^5$	$k_4 \times 10^6$
1·1140	0·3458	0·499	−0·21	−0·03
1·1160	0·3244	0·534	−0·24	−0·07
1·1180	0·3236	0·425	−0·84	0·22
1·1200	0·2907	0·629	−0·62	0·04
1·1210	0·2508	1·633	−2·58	−0·08
1·1220	0·2008	6·075	−26·95	−32·38
1·1230	0·1995	4·047	−30·99	16·89
1·1235	0·2131	4·496	−31·79	19·35
1·1238	0·1482	5·530	−1·19	−24·79
1·1240	0·0711	5·498	30·52	−10·72
1·1250	0·0539	2·073	1·13	−2·34
1·1260	0·0273	0·966	0·44	−0·59
1·1270	0·0283	1·275	0·33	−0·50
1·1280	0·0288	2·073	9·62	3·14
1·1290	0·0194	1·146	2·65	0·13
1·1300	0·0123	0·605	0·03	0·01
1·1320	0·0088	0·781	1·75	0·53
1·1340	0·0081	0·544	−0·03	−0·11
1·1360	0·0088	0·477	0·10	−0·02
1·1380	0·0110	0·623	0·59	0·00
1·1400	0·0046	0·337	0·05	−0·03
1·1600	0·0031	0·249	0·06	−0·02
1·1800	0·0019	0·168	0·04	0·00
1·2000	0·0013	0·119	0·00	0·00
1·2500	0·0007	0·075	0·01	0·00
1·3000	−0·0003	0·060	0·00	0·00

we estimate the two order parameters at the transition to be 0·27 and 0·25 for $\langle P_2\rangle_\lambda$ and $\langle P_2\rangle_{\lambda_2}$ respectively.

We now turn to an algorithm for the determination of the fourth rank order parameter $\langle P_4\rangle$. To this end let us consider the fourth rank tensor $\mathbf{F}$, where $\mathbf{F} = \mathbf{A} \times \mathbf{A}$, the direct product of the second rank quantity $\mathbf{A}$ introduced earlier on. The sample average of $\mathbf{F}$ in the laboratory frame is related to that in the director frame previously defined through a similarity transformation employing the matrix $\mathbf{U}$ of the $\langle \mathbf{A}^{\mathrm{L}}\rangle_{\mathrm{S}}$ eigenvectors

$$\langle \mathbf{F}^{\mathrm{L}}\rangle_{\mathrm{S}} = \langle \mathbf{A}^{\mathrm{L}} \times \mathbf{A}^{\mathrm{L}}\rangle_{\mathrm{S}}, \tag{11 a}$$

$$= \langle (\mathbf{U}\mathbf{A}^{\mathrm{D}}\tilde{\mathbf{U}}) \times (\mathbf{U}\mathbf{A}^{\mathrm{D}}\tilde{\mathbf{U}})\rangle_{\mathrm{S}}, \tag{11 b}$$

$$= (\mathbf{U} \times \mathbf{U})\langle \mathbf{A}^{\mathrm{D}} \times \mathbf{A}^{\mathrm{D}}\rangle_{\mathrm{S}}(\tilde{\mathbf{U}} \times \tilde{\mathbf{U}}), \tag{11 c}$$

$$= (\mathbf{U} \times \mathbf{U})\langle \boldsymbol{F}^{\mathrm{D}}\rangle_{\mathrm{S}}(\tilde{\mathbf{U}} \times \tilde{\mathbf{U}}). \tag{11 d}$$

The average of $\mathbf{F}$ in the director frame is related in turn to the molecule fixed components as

$$\langle \mathbf{A}^{\mathrm{D}} \times \mathbf{A}^{\mathrm{D}}\rangle_{\mathrm{S}} = \langle (\mathbf{R}\mathbf{A}^{\mathrm{M}}\tilde{\mathbf{R}}) \times (\mathbf{R}\mathbf{A}^{\mathrm{M}}\tilde{\mathbf{R}})\rangle \tag{12 a}$$

$$= (\mathbf{R} \times \mathbf{R})\langle \mathbf{A}^{\mathrm{M}} \times \mathbf{A}^{\mathrm{M}}\rangle_{\mathrm{S}}(\tilde{\mathbf{R}} \times \tilde{\mathbf{R}}) \tag{12 b}$$

$$= (\mathbf{R} \times \mathbf{R})\langle \mathbf{F}^{\mathrm{M}}\rangle_{\mathrm{S}}(\tilde{\mathbf{R}} \times \tilde{\mathbf{R}}) \tag{12 c}$$

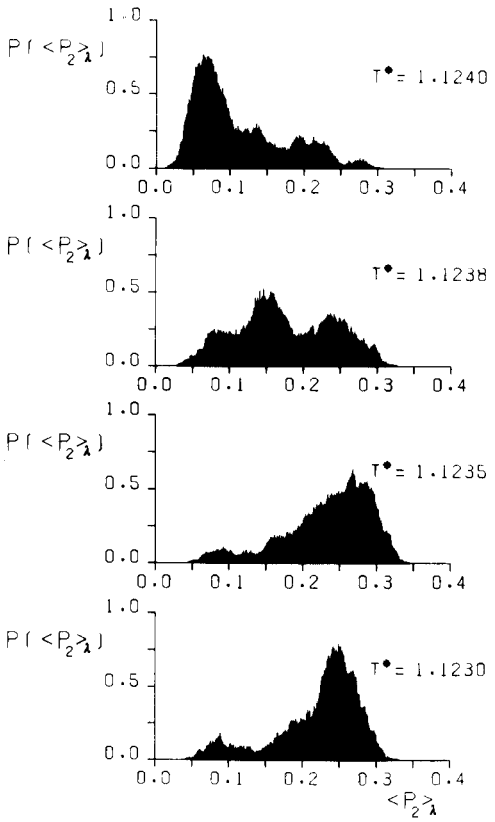

Figure 5. Histograms of the distribution of second rank order parameters $\langle P_2 \rangle_\lambda$ obtained during the simulation at four temperatures T^* in the neighbourhood of the transition.

Since $\mathbf{F}^{\mathrm{M}}$ is a constant and $F^{\mathrm{M}}_{ijkl} = \delta_{iz}\delta_{jz}\delta_{kz}\delta_{lz}$, the component F_{ZZZZ} in the director frame of this tensor becomes

$$\begin{aligned} \langle F^{\mathrm{D}}_{ZZZZ} \rangle_{\mathrm{S}} &= \langle (\mathbf{R}_{ZZ})^4 \rangle_{\mathrm{S}}, \\ &= \langle \cos^4 \beta \rangle_{\mathrm{S}}, \end{aligned} \tag{13}$$

which can be used, together with $\langle P_2 \rangle_{\mathrm{S}}$ to determine $\langle P_4 \rangle_{\mathrm{S}}$.

$$\langle P_4 \rangle_{\mathrm{S}} = \frac{35}{8}\langle \cos^4 \beta \rangle_{\mathrm{S}} - \frac{30}{8}\langle \cos^2 \beta \rangle_{\mathrm{S}} + \frac{3}{8}. \tag{14}$$

The relevant component in the director frame is determined by first calculating at every cycle the sample average of the tensor $\mathbf{F}$ in the laboratory frame as

$$\langle F^{\mathrm{L}}_{abcd} \rangle_{\mathrm{S}} = \langle q_a q_b q_c q_d \rangle_{\mathrm{S}} \tag{15}$$

then rotating to a director frame employing the previously determined eigenvectors matrix of $\mathbf{A}$.

$$\langle F^{\mathrm{D}}_{ZZZZ} \rangle_{\mathrm{S}} = \sum_{a,b,c,d} U_{aZ} U_{bZ} U_{cZ} U_{dZ} \langle F^{\mathrm{L}}_{abcd} \rangle_{\mathrm{S}} \tag{16}$$

This quantity is then averaged over the cycles to produce the calculated $\langle P_4 \rangle_\lambda$. Notice that, differently from a previously proposed algorithm [4] the present one preserves the information about the sign of $\langle P_4 \rangle$. We do not actually expect a negative fourth rank order parameter for the Lebwohl–Lasher model but this could be the case for other more complex interactions, so the possibility should certainly be allowed for. This is particularly important in view of the debate about the sign of $\langle P_4 \rangle$ which has followed some experimental determinations of negative values of $\langle P_4 \rangle$ [37]. The values for the fourth rank order parameter obtained for our simulation are reported as a function of temperature in figure 6. The distribution of the fourth rank order parameters values observed in the course of the simulation has also been determined and in table 4 we reproduce a summary of the results. The histograms of $\langle P_4 \rangle_\lambda$ in the transition region show a clear two peaks behaviour (cf. figure 7). We estimate $\langle P_4 \rangle_\lambda$ at the transition to be 0·04, both from inspection of the histograms in figure 7 and from figure 6.

In figure 8 we plot our results for $\langle P_4 \rangle$ against $\langle P_2 \rangle$ since there are definite predictions in the literature for this curve. We report first (curve A) a simple approximation proposed by Faber [16] i.e. $\langle P_4 \rangle = \langle P_2 \rangle^{10/3}$. This relationship follows from its proposed continuum theory of disordering by fluctuations in a lattice model like the present one. The relation has a strikingly simple form and

Table 4. The first four cumulants, k_1, k_2, k_3, k_4 of the distribution $P(\langle P_4 \rangle_\lambda)$ of the fourth rank order parameter values observed during the Monte Carlo simulations at temperatures T^*.

T^*	k_1	$k_2 \times 10^4$	$k_3 \times 10^6$	$k_4 \times 10^8$
1·1140	0·0659	0·710	0·22	0·2
1·1160	0·0580	0·684	0·08	−0·1
1·1180	0·0583	0·496	−0·03	−0·1
1·1200	0·0472	0·608	−0·04	−0·2
1·1210	0·0368	1·143	0·13	0·3
1·1220	0·0271	2·321	−0·72	−5·9
1·1230	0·0262	1·322	−0·62	−0·5
1·1235	0·0290	1·675	−0·44	−1·6
1·1238	0·0178	1·498	1·04	−1·0
1·1240	0·0082	0·901	1·11	1·2
1·1250	0·0052	0·248	0·04	0·0
1·1260	0·0027	0·142	0·01	0·0
1·1270	0·0026	0·168	0·02	0·0
1·1280	0·0030	0·233	0·09	0·1
1·1290	0·0019	0·142	0·01	0·0
1·1300	0·0016	0·113	0·01	0·0
1·1320	0·0009	0·117	0·01	0·0
1·1340	0·0011	0·106	0·00	0·0
1·1360	0·0009	0·100	0·00	0·0
1·1380	0·0007	0·100	0·01	0·0
1·1400	0·0006	0·097	0·00	0·0
1·1600	0·0002	0·072	0·00	0·0
1·1800	−0·0001	0·068	0·00	0·0
1·2000	−0·0002	0·062	0·00	0·0
1·2500	−0·0004	0·056	0·00	0·0
1·3000	−0·0004	0·053	0·00	0·0

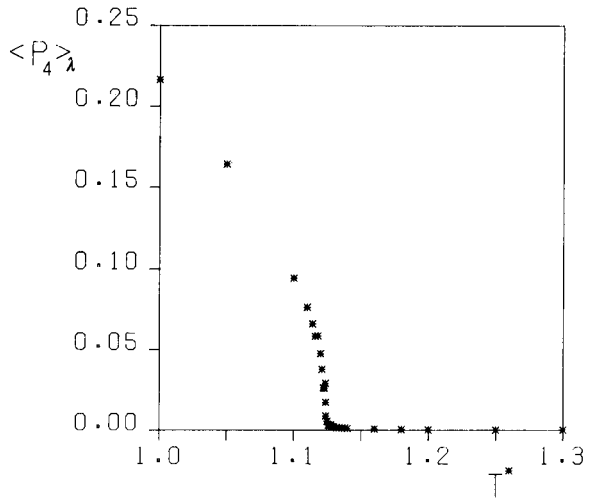

Figure 6 The fourth rank order parameter $\langle P_4 \rangle_\lambda$ obtained as described in the text plotted vs. temperature T^*.

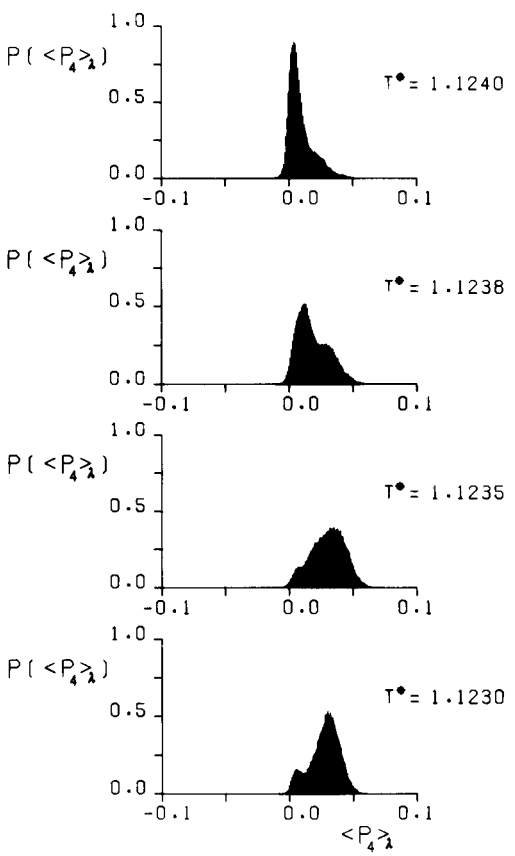

Figure 7. The distribution of fourth rank order parameters $\langle P_4 \rangle_\lambda$ occurring during the simulations at a few temperatures in the vicinity of the orientational transition.

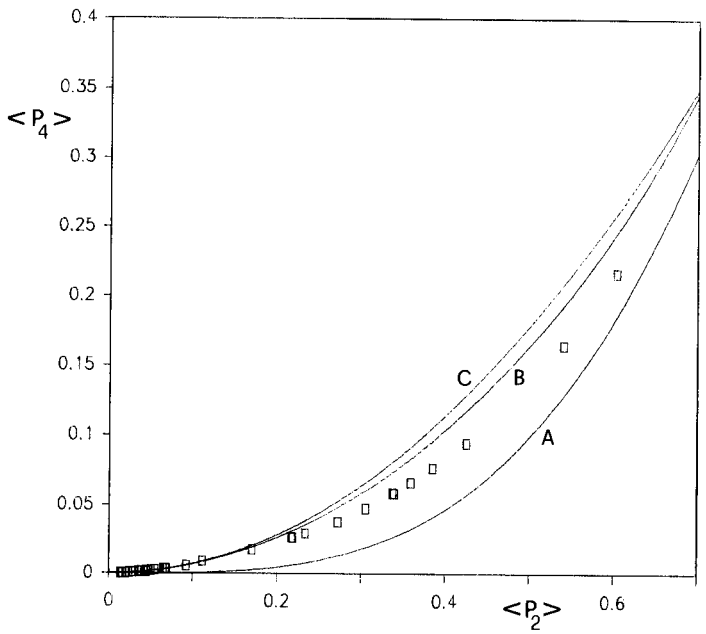

Figure 8. The fourth rank order parameter $\langle P_4 \rangle$ plotted versus the second rank one $\langle P_2 \rangle$. Here the open squares are the simulation results for $\langle P_2 \rangle_\lambda$. Curve (A) is $\langle P_2 \rangle^{(10/3)}$ as from Faber's theory [16]. Curve (B) is obtained from mean field or in general from the distribution in equation (17). Curve (C) is the simple approximation $\frac{5}{7}\langle P_2 \rangle^2$ to curve (B).

represents $\langle P_4 \rangle$ vs. $\langle P_2 \rangle$ well when the order is high [16]. Here it is definitely lower than the experimental values, although it starts to approach them at our higher values of $\langle P_2 \rangle$ i.e. 0·6. A molecular alternative to obtaining a relation between $\langle P_4 \rangle$ and $\langle P_2 \rangle$ requires an orientational singlet distribution. In particular we consider the single particle distribution (see, e.g., 14)

$$P(\cos \beta) = \frac{1}{Z(a_2)} \exp [a_2 P_2(\cos \beta)], \tag{17}$$

where $Z(a_2)$ is a normalization factor. In mean field the coefficient a_2 is $a_2 = (z/T^*)\langle P_2 \rangle$ for the present model, with $z = 6$ being the coordination number. However, a second rank effective potential like that implicit in equation (17) could be obtained by other means. For example this particular form can be deduced by constructing the maximum entropy [38] singlet distribution from $\langle P_2 \rangle$ information or by truncating some general expansion of the unknown true potential of mean torque at the first non trivial term. In any case, given this distribution, $\langle P_2 \rangle$ and $\langle P_4 \rangle$ can be obtained as functions of the interaction strength parameter a_2 by applying equation (8) for both $L = 2$ and $L = 4$. Elimination of the parameter a_2 between the resulting equations for $\langle P_2 \rangle$ and $\langle P_4 \rangle$ then yields the universal curve plotted as (B) in figure 8. This curve is unfortunately not susceptible to a straightforward analytical formulation. We can, however, obtain a simple approximation as follows. First a series expansion of a_2

in terms of $\langle P_2 \rangle$ gives

$$a_2 = 5\langle P_2\rangle - \frac{25}{7}\langle P_2\rangle^2 + \frac{425}{49}\langle P_2\rangle^3 - \frac{51875}{3773}\langle P_2\rangle^4 + \frac{1419625}{49049}\langle P_2\rangle^5 - \frac{1721875}{31213}\langle P_2\rangle^6 + \frac{356380553125}{3146051909}\langle P_2\rangle^7 + \ldots . \quad (18)$$

The series is of course divergent at $\langle P_2 \rangle = 1$, since we know that getting $\langle P_2 \rangle = 1$ requires $a_2 \to \infty$ but it can still be used [39] for our purposes for the present range of order parameters. It is interesting to note that the trivial first term,

$$a_2 = 5\langle P_2\rangle \quad (19)$$

is a simple approximation with an error of less than 30 per cent for $\langle P_2 \rangle$ smaller than 0·4 i.e. for order parameters not too far from the transition. Expanding $\langle P_4 \rangle$ in terms of a_2 (up to order seven here) and substituting a_2 from (18) gives a series for $\langle P_4 \rangle$ in terms of $\langle P_2 \rangle$

$$\langle P_4\rangle = \frac{5}{7}\langle P_2\rangle^2 - \frac{200}{539}\langle P_2\rangle^3 + \frac{35650}{49049}\langle P_2\rangle^4 - \ldots . \quad (20)$$

The series contains large terms of alternating sign and is poorly convergent unless terms are properly grouped together [39]. The very simplest grouping consist of retaining just the first term,

$$\langle P_4\rangle = \frac{5}{7}\langle P_2\rangle^2, \quad (21)$$

which actually gives quite a good approximation to curve (B) at least up to order parameter $\langle P_2 \rangle = 0{\cdot}6$. This approximation is reported as curve (C) in figure 8.

3.5. *Pair properties*

The rotationally invariant pair distribution $G(r_{12}, \omega_{12})$ [8, 23] determines the probability of finding two particles at distance r_{12} with a certain relative orientation ω_{12}. It is convenient to expand $G(r_{12}, \omega_{12})$ in a series of Legendre polynomials as

$$G(r_{12}, \omega_{12}) = G_0^{00}(r_{12}) \sum_L [(2L+1)/64\pi^4] G_L(r_{12}) P_L(\cos \beta_{12}) \quad (22)$$

for even L, where $G_0^{00}(r_{12})$ is a purely scalar radial distribution and the expansion coefficients define two-particles order parameters. These in turn give the correlation between the orientation of two particles separated by a distance r_{12}.

$$G_L(r_{12}) = [1/G_0^{00}(r_{12})] \int d\omega_1 \, d\omega_2 \, G(r_{12}, \omega_{12}) P_L(\cos \beta_{12}) = \langle P_L(\cos \beta_{12}) \rangle_{r_{12}}. \quad (23)$$

For our lattice system the particle positions are fixed and the centres distribution is just

$$G_0^{00}(r_{12}) = [1/(4\pi r_{12}^2 \rho)] \sum_k z_k \delta(r_{12} - r_k), \quad (24)$$

where ρ is the number density and the sum runs over successive shells containing z_k neighbours at distance r_k from the central particle. Here r is in lattice units.

We have calculated the angular pair correlation coefficients $G_L(r)$ [6] for rank $L = 2$ and 4. In figure 9 (*a*) (*b*) we show $G_2(r)$ and $G_4(r)$ for a number of temperatures from $T^* = 1{\cdot}05$ to $1{\cdot}20$ of the $30 \times 30 \times 30$ system. When using periodic boundary conditions, every distance dependent property is determined modulo the box length so the correlations grow for distances exceeding half the box length. Here we show the curves for r starting from the nearest neighbour distance up to two thirds of the box length to show the relative unimportance of the build-up at these distances. The pair coefficients $G_L(r)$ should start from one and tail off to essentially $\langle P_L \rangle^2$ in the nematic phase [8]. We have checked that this is indeed the case for our simulation. The various curves are plotted together to yield an overall impression of the temperature-distance surface and the trivial starting point $G_L(0) = 1$ has been omitted for clarity. The build-up of the orientational correlation when approaching the transition from above is quite visible and will be examined in detail. In figure 10 we plot a number of sections of the $G_2(r)$ vs. temperature surface at selected distances. A line joining the points is drawn as a guide to the eye. The various curves show the difference in the permanence of short range order at nearest neighbour distance (squares) even above the transition and the rather fast approach to long range type behaviour when the interparticle separation exceeds five or six lattice spacings. As seen from equation 22 the correlation coefficients $G_L(r)$ represent the first few terms in the pair distribution expansion. Even though the distribution in itself may be slowly convergent, the first few coefficients cover an important role, as we can see by considering a generic pairwise additive property A,

$$A = \sum_{i,j} A(r_{ij}, \omega_{ij}), \tag{25}$$

where $A(r_{ij}, \omega_{ij})$ is a function of relative orientation and position between two particles. In particular, if the quantity A is a sum of a finite number of terms of different rank J

$$A(r_{12}, \omega_{12}) = \sum_J a_J(r_{12}) D^J_{00}(\omega_{12}), \tag{26}$$

the average of A is just

$$\langle A \rangle = N \sum_k \sum_J z_k a_J(r_k) G_J(r_k) \tag{27}$$

where z_k is the number of neighbours at a distance r_k from the particle at the origin. As a simple special case we recover the average energy equation (3 *b*). We shall employ the correlation coefficients in investigating pretransitional behaviour in our system.

3.6. *Pretransitional behaviour*

Large ordering effects are known to take place in nematogen materials above the isotropic transition. These pretransitional effects are of great importance in liquid crystals and have been observed, e.g. through electric [40] and magnetic [23] birefringence as well as by light scattering [41]. A particularly neat demonstration through N.M.R. detected magnetic field effect has been recently given by the Southampton group [42]. An N.M.R. detected Kerr effect has been reported

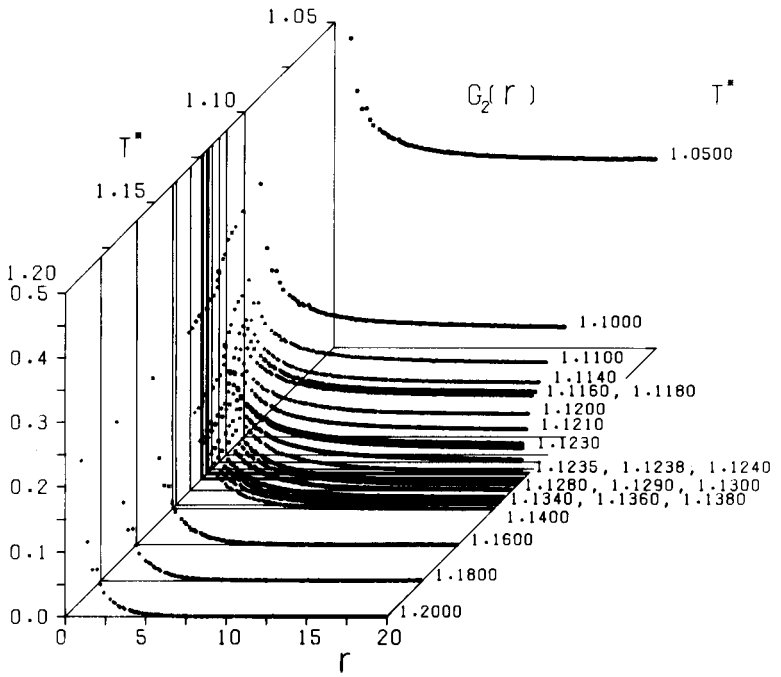

(*a*)

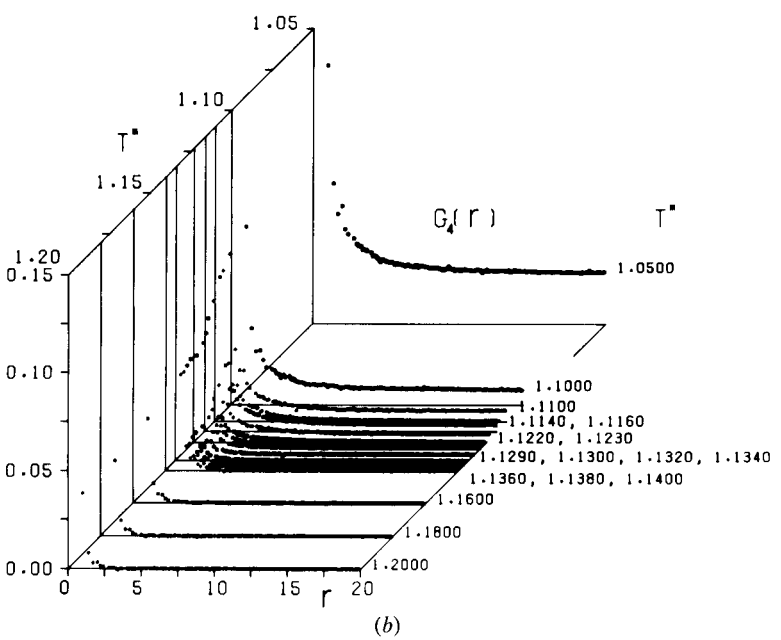

(*b*)

Figure 9. (*a*) The spatial correlation function $G_2(r)$ at various temperatures below and above the transition. Here we show results for a range of temperature T^* as indicated on the graph. The distance r is measured in lattice units. (*b*) The fourth rank correlation $G_4(r)$ at the same temperatures.

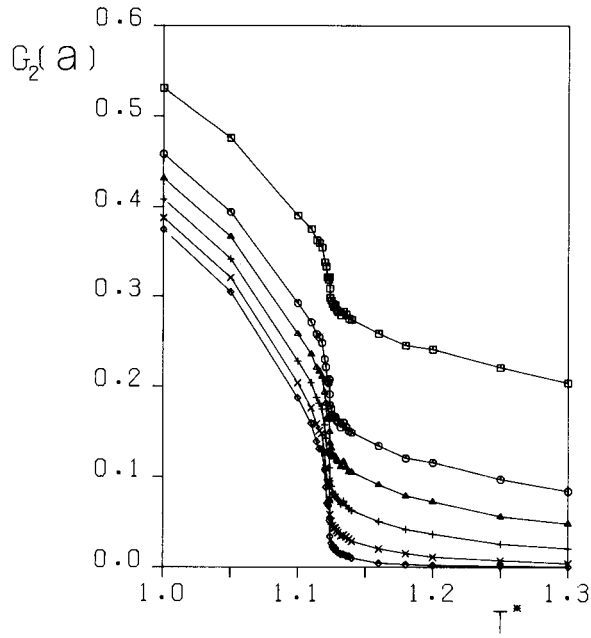

Figure 10. Sections of the $G_2(r, T^*)$ surface at six selected distances $r = a$. Here $a = 1$ (□), 1·4 (○), 1·7 (△), 2·4 (+), 3·7 (×), 5·9 (◇).

by MacLean *et al.* [43]. A particularly significant finding in all these experiments is that the temperature of divergence of these pretransitional effects is not the transition temperature but a slightly lower one $T^*_{NI^*}$. The conventional wisdom is that a hypothetical second order phase transition, which would occur at $T^*_{NI^*}$, is preempted by a first order transition. Here we wish to study pretransitional effects through simulations and we start by obtaining the relevant equations for the susceptibility, in the isotropic phase and introduce the prescription we have used for its computation. We consider the ordering induced by a uniform field which contributes to the system hamiltonian a perturbation term H',

$$H' = \lambda B^2 \phi(\beta_1, \beta_2, \ldots, \beta_N), \tag{28}$$

where B^2 is the intensity of the field, e.g. magnetic and λ represents the effectiveness of coupling between the field and each molecule with orientation β_i. We assume a uniform field with λ constant and a second rank anisotropic part

$$\phi = \sum_{i=1}^{N} P_2(\cos \beta_i). \tag{29}$$

The order parameter in the presence of the field is

$$\langle P_2 \rangle_{T,B} = \frac{1}{N} \langle \phi \rangle_{T,B}, \tag{30 a}$$

$$= \frac{1}{Z(T, B)} \int \phi \exp\left[(U + H')/kT\right] d\mathbf{X}_1 \, d\mathbf{X}_2 \ldots d\mathbf{X}_N, \tag{30 b}$$

where $d\mathbf{X}$ is the orientational volume element and $Z(T, B)$ is the configurational integral normalizing the right hand side of equation (30 *b*). In a linear regime the

order parameter induced by the field is just proportional to the strength of the applied field itself through a susceptibility κ, i.e.

$$\langle P_2 \rangle_{T,B} = \kappa B^2, \tag{31}$$

where the field susceptibility κ is the derivative

$$\kappa = \frac{\partial}{\partial B^2} \langle P_2 \rangle_{T,B=0} \tag{32}$$

evaluated at zero field. The susceptibility can thus be rewritten as

$$\kappa = (\lambda/NkT)\{\langle \phi^2 \rangle_{B=0} - \langle \phi \rangle^2_{B=0}\}, \tag{33 a}$$

$$= (\lambda/NkT)\left\{\sum_i \sum_j \langle P_2(\cos \beta_i) P_2(\cos \beta_j) \rangle_{B=0}\right\}. \tag{33 b}$$

To obtain equation (33 *b*) we have used the fact that in the isotropic phase the unperturbed order parameter is zero. The two particle average in equation (33 *b*) can be rewritten in terms of $G_2(r)$ using equations (27) and (22). Thus we obtain

$$\langle P_2(\cos \beta_1) P_2(\cos \beta_2) \rangle = (1/V) \int d\mathbf{r}_{12}\, d\omega_{12}\, G(r_{12}, \omega_{12}) P_2(\cos \beta_1) P_2(\cos \beta_2), \tag{34 a}$$

$$= \frac{1}{5V} \int dr\, r^2 G_0^{00}(r) G_2(r), \tag{34 b}$$

$$= \frac{1}{5N} g_2, \tag{34 c}$$

where the coefficient g_2 is defined as the zero field average

$$g_2 = \frac{5}{N} \sum_i \sum_j \langle P_2(\cos \beta_i) P_2(\cos \beta_j) \rangle_{B=0}. \tag{35}$$

The susceptibility κ then becomes

$$\kappa = (\lambda/kT) g_2. \tag{36}$$

The quantity g_2 contains the molecular information on the existing orientational pair correlations and is sometimes called a second rank Kirkwood coefficient [6] by analogy with the first rank dipolar correlation coefficients introduced in the study of dielectric properties [44]. For our lattice system g_2 can be conveniently formulated using equation (24) for $G_0^{00}(r)$. We find

$$g_2 = \sum_k z_k G_2(r_k) \tag{37}$$

which is the expression we have actually used to compute g_2 from our simulation data. The divergence temperature can then be determined by fitting T^*/g_2 vs. T^* [6]. Truncating the sum at $r_k = 15$, a good linear fit with a correlation coefficient of 0·997 is obtained. The intercept gives the divergence at $T^*_{NI^*} = 1{\cdot}118 \pm 0{\cdot}004$. Evaluation of g_2 through the sum formula in equation (37) has the advantage over direct summation over the whole sample [6] that spurious contributions to g_2 due to the build up of the correlation at distances comparable to the box length are controllable by suitably truncating the sum. However, the number of neighbours increases quadratically with distance and it is worth checking if the results are

dependent on the arbitrary cut-off distance imposed. This was found to be an important factor in determinations of g_2 for relatively small isotropic samples [45]. In order to try and eliminate this cut-off effect we have sought to use our data to determine the parameters in a suitable analytic model for the distance decay of $G_2(r)$. If this can be done the analytic expression can then be used in conjunction with equation (37) to estimate the neglected tail contributions to g_2. We have fitted various models for the decay of correlation with separation to the experimental $G_2(r)$ for temperatures greater than 1·1238, limiting r to be smaller than a cut-off length of respectively 10, 15 and 20 lattice units. The models ranged from a simple exponential decay to zero or to a plateau to the classical Ornstein–Zernike form [23, 46],

$$G_2(r) = \frac{A}{r} \exp(-k_c r), \tag{38}$$

where k_c has the meaning of an inverse correlation length. We have found the Ornstein–Zernike form to yield an excellent overall fit at the various temperatures. Moreover essentially the same parameters A and k_c are obtained from the different truncations assumed. The results for the inverse correlation length k_c are reproduced with different symbols (+, ○, ×) for the three truncations in figure 11. It is interesting to notice that an Orstein–Zernike form is expected theoretically and that Landau–de Gennes theory predicts that the correlation length squared should be linear in temperature. In figure 12 we show that this is indeed the case. The temperature of divergence of the correlation length is found to be in this way $T^* = 1{\cdot}1222 \pm 0{\cdot}009$. As a further step we can now substitute the Ornstein–Zernike form for $G_2(r)$ in equation (37) and extend the sum up to arbitrary large distances until convergence fails. As a first check we have used the Ornstein–Zernike expression and truncated the sum at $r = 15$ and we have found that the results for the divergence temperature of g_2 ($T^* = 1{\cdot}118$) previously given are recovered. We have then considered distances up to $r = 150$. The g_2 calculated in this way are of course independent of cut off. Using these values we

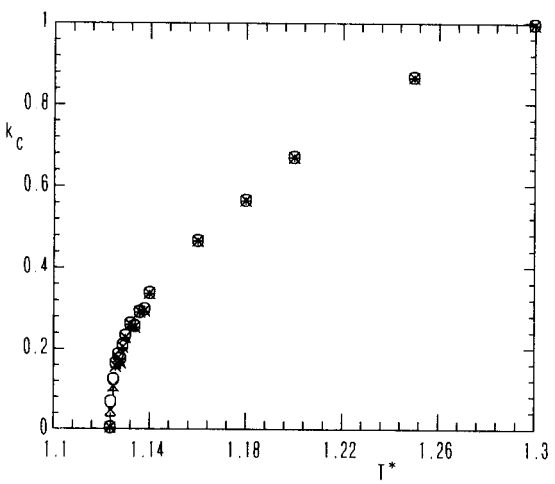

Figure 11. The inverse correlation length k_c as obtained by fitting the Ornstein–Zernike expression to the $G_2(r)$ vs. r data for T^* greater than 1·1238. Fits for data up to reduced distances $r = 10$ (+), 15 (○) and 20 (*) are shown.

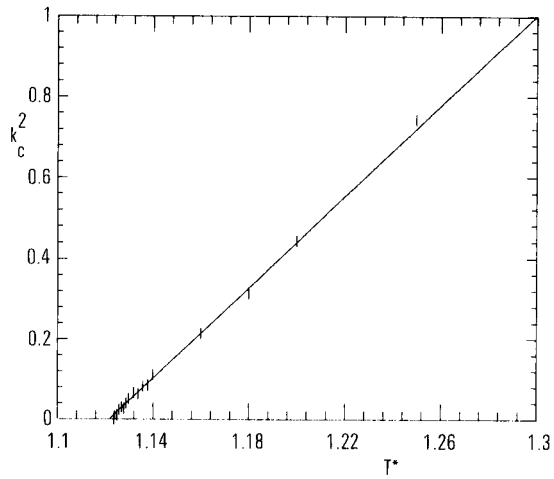

Figure 12. The square of the inverse correlation length k_c (*) vs temperature plotted together with its linear regression line.

can compute corrected values for T^*/g_2 and by performing once again a linear regression in temperature (shown in figure 13) we find our final estimate for the divergence temperature

$$T^*_{\mathrm{NI}^*} = 1{\cdot}1201 \pm 0{\cdot}0006.$$

Thus inclusion of long range corrections to g_2 brings the divergence point nearer to the transition temperature. It was argued that the LL model could not give these two temperatures close enough but this does not seem to be the case. Translating to real temperatures the difference in T_{NI} and T_{NI^*} for the Lebwohl–Lasher model is ~ 1 K which is in agreement with experiment.

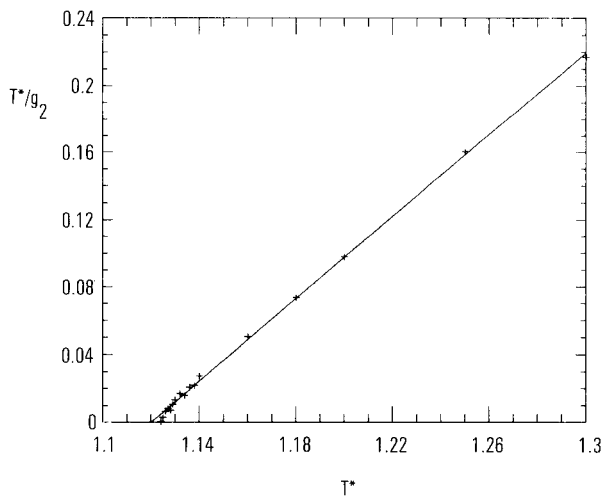

Figure 13. Linear regression of the inverse g_2 obtained from summation of the Ornstein–Zernike fitted expression, T^*/g_2, vs. temperature T^*.

4. Discussion and conclusions

We have determined the transitional and pretransitional properties of this important model of liquid crystals to an accuracy greater than previously possible. Our transition temperature is slightly less than that found by Lebwohl–Lasher [1] and Luckhurst and Simpson [7] in accord with the idea that in systems with periodic boundary conditions the transition is approached from above, so that going to larger systems lowers the temperature at which the heat capacity has its maximum.

According to the simulation results the simple Lebwohl–Lasher model can provide all the important characteristics of the transition, including the correct order of magnitude of the deviation of T^*_{NI} from the nematic–isotropic transition temperature. This is in our view a particularly significant result, which points to the need to refining the theoretical approaches employed to treat this class of problems.

We are grateful to Dr. M. Lanzarini (CINECA) for his support to this project and to CINECA for the generous allocation of time on the CRAY which made this work possible. C. Z. thanks Min. P. I. and C. N. R. for financial support.

Appendix

Table A 1. A summary of our results for the Monte Carlo simulation on the 30 × 30 × 30 Lebwohl–Lasher model. Here N_c is the total number of cycles in the simulation. The symbols and the errors have been described in the text.

T^*	$\langle U^* \rangle$	$\langle P_2 \rangle_\lambda$	$\langle P_2 \rangle_{\lambda_2}$	$\langle P_4 \rangle_\lambda$	C_V^*	$N_c/1000$
1·0000	−1·5867 ± 0·0007	0·6038 ± 0·0008	0·5972 ± 0·0005	0·2164 ± 0·00086	3·03 ± 0·027	10
1·0500	−1·4240 ± 0·0008	0·5405 ± 0·0011	0·5334 ± 0·0015	0·1645 ± 0·00099	3.71 ± 0·048	10
1·1000	−1·1879 ± 0·0017	0·4250 ± 0·0012	0·4148 ± 0·0008	0·0946 ± 0·00079	6·07 ± 0·229	10
1·1100	−1·1211 ± 0·0037	0·3848 ± 0·0040	0·3732 ± 0·0027	0·0768 ± 0·00196	7·69 ± 0·063	10
1·1140	−1·0846 ± 0·0033	0·3590 ± 0·0031	0·3463 ± 0·0033	0·0664 ± 0·00118	8·61 ± 0·021	13
1·1160	−1·0647 ± 0·0035	0·3391 ± 0·0035	0·3247 ± 0·0036	0·0586 ± 0·00127	9·84 ± 0·225	14
1·1180	−1·0557 ± 0·0015	0·3375 ± 0·0032	0·3241 ± 0·0047	0·0588 ± 0·00166	13·95 ± 0·518	10
1·1200	−1·0220 ± 0·0033	0·3056 ± 0·0039	0·2912 ± 0·0045	0·0477 ± 0·00126	20·14 ± 0·499	15
1·1210	−0·9946 ± 0·0048	0·2727 ± 0·0063	0·2540 ± 0·0072	0·0380 ± 0·00177	22·70 ± 0·240	20
1·1220	−0·9578 ± 0·0093	0·2173 ± 0·0154	0·1950 ± 0·0169	0·0265 ± 0·00324	24.00 ± 0·231	25
1·1230	−0·9540 ± 0·0049	0·2188 ± 0·0086	0·1966 ± 0·0096	0·0263 ± 0·00160	24·44 ± 0·767	50
1·1235	−0·9617 ± 0·0045	0·2336 ± 0·0073	0·2132 ± 0·0082	0·0294 ± 0·00152	24·40 ± 0·980	70
1·1238	−0·9217 ± 0·0045	0·1702 ± 0·0081	0·1433 ± 0·0091	0·0175 ± 0·00145	24·03 ± 1·055	70
1·1240	−0·8955 ± 0·0037	0·1115 ± 0·0080	0·0734 ± 0·0094	0·0090 ± 0·00117	23·54 ± 1·068	70
1·1250	−0·8812 ± 0·0025	0·0923 ± 0·0059	0·0544 ± 0·0068	0·0057 ± 0·00057	19·63 ± 0·885	30
1·1260	−0·8704 ± 0·0021	0·0652 ± 0·0047	0·0278 ± 0·0047	0·0032 ± 0·00038	14·70 ± 0·509	25
1·1270	−0·8651 ± 0·0015	0·0675 ± 0·0038	0·0288 ± 0·0051	0·0031 ± 0·00039	10·31 ± 0·181	25
1·1280	−0·8646 ± 0·0026	0·0693 ± 0·0069	0·0293 ± 0·0083	0·0035 ± 0·00069	7·21 ± 0·030	25
1·1290	−0·8558 ± 0·0018	0·0555 ± 0·0046	0·0199 ± 0·0052	0·0024 ± 0·00034	5·27 ± 0·011	25
1·1300	−0·8498 ± 0·0016	0·0502 ± 0·0030	0·0128 ± 0·0038	0·0021 ± 0·00029	4·02 ± 0·011	15
1·1320	−0·8445 ± 0·0012	0·0450 ± 0·0041	0·0093 ± 0·0050	0·0014 ± 0·00030	2·87 ± 0·009	15
1·1340	−0·8377 ± 0·0019	0·0456 ± 0·0037	0·0086 ± 0·0029	0·0016 ± 0·00028	2·78 ± 0·054	15
1·1360	−0·8304 ± 0·0014	0·0389 ± 0·0024	0·0093 ± 0·0034	0·0014 ± 0·00026	2·86 ± 0·109	15
1·1380	−0·8256 ± 0·0013	0·0428 ± 0·0032	0·0115 ± 0·0042	0·0012 ± 0·00025	2·90 ± 0·125	15
1·1400	−0·8187 ± 0·0010	0·0353 ± 0·0012	0·0051 ± 0·0018	0·0011 ± 0·00019	2·84 ± 0·119	15
1·1600	−0·7747 ± 0·0005	0·0289 ± 0·0009	0·0036 ± 0·0011	0·0007 ± 0·00013	1·87 ± 0·016	15
1·1800	−0·7401 ± 0·0006	0·0239 ± 0·0010	0·0024 ± 0·0011	0·0004 ± 0·00006	1·57 ± 0·008	15
1·2000	−0·7117 ± 0·0003	0·0198 ± 0·0005	0·0018 ± 0·0005	0·0003 ± 0·00005	1·31 ± 0·013	15
1·2500	−0·6542 ± 0·0003	0·0158 ± 0·0002	0·0012 ± 0·0005	0·0001 ± 0·00004	1·00 ± 0·003	15
1·3000	−0·6090 ± 0·0002	0·0137 ± 0·0003	0·0002 ± 0·0002	0·0001 ± 0·00005	0·86 ± 0·004	15

References

[1] Lebwohl, P. A., and Lasher, G., 1972, *Phys. Rev.* A, **6,** 426.
[2] Meirovitch, H., 1976, *Chem. Phys.*, **21,** 251.
[3] Jansen, H. J. F., Vertogen, G. and Ypma, J. G. J., 1977, *Molec. Crystals liq. Crystals*, **38,** 87.
[4] Zannoni, C., 1979, *The Molecular Physics of Liquid Crystals*, edited by G. R. Luckhurst and G. W. Gray (Academic Press), (a) Chap. 3, (b) Chap. 9.
[5] Zannoni, C., and Guerra, M., 1981, *Molec. Phys.*, **44,** 849.
[6] Humphries, R. L., and Luckhurst, G. R., 1982, *Proc. R. Soc.* A, **382,** 307.
[7] Luckhurst, G. R. and Simpson, P., 1982, *Molec. Phys.*, **47,** 251.
[8] Zannoni, C., 1986, *J. chem. Phys.*, **84,** 424.
[9] Maier, W., and Saupe, A., 1958, *Z. Naturf.* A, **13,** 564.
[10] Vuillermot, P. A., and Romerio, M. V., 1973, *J. Phys.* C, **6,** 2922.
[11] Sheng, P., and Wojtowicz, P. J., 1976, *Phys. Rev.* A, **14,** 1883.
[12] Ypma, J. G. J., Vertogen, G., and Koster, H. T., 1976, *Molec. Crystals liq. Crystals*, **37,** 57.
[13] Madhusudana, N. V., Savithramma, K. L., and Chandrasekhar, S., 1977, *Pramana*, **8,** 22.
[14] Luckhurst, G. R., 1979, *The Molecular Physics of Liquid Crystals*, edited by G. R. Luckhurst and G. W. Gray (Academic Press), Chap. 4.
[15] Van der Haegen, R., Debruyne, J., Luyckx, R., and Lekkerkerker, H. N. W., 1980, *J. chem. Phys.*, **73,** 2469.
[16] Faber, T. E., 1980, *Proc. R. Soc.* A, **370,** 509; 1984, *Ibid.*, **396,** 357.
[17] Shukla, P., and Sluckin, T. J., 1985, *J. Phys.* A, **18,** 93.
[18] Landau, D. P., 1984, *Applications of the Monte Carlo Method in Statistical Physics*, edited by K. Binder (Springer-Verlag), Chap. 3, and references therein.
[19] Mouritsen, O. G., 1984, *Computer Studies of Phase Transitions and Critical Phenomena* (Springer-Verlag).
[20] Binder, K., 1979, *Monte Carlo Methods in Statistical Physics*, edited by K. Binder (Springer-Verlag), p. 1, and references therein.
[21] Binder, K., 1985, *J. Computat. Phys.*, **59,** 1.
[22] see, e.g. Thoen, J., Marynissen, H., and Van Dael, W., 1982, *Phys. Rev.* A, **26,** 2886.
[23] De Gennes, P. G., 1974, *The Physics of Liquid Crystals* (Clarendon Press).
[24] Stinson, T. W., and Litster, J. D., 1970, *Phys. Rev. Lett.*, **25,** 503.
[25] Chandrasekhar, S., 1977, *Liquid Crystals* (Cambridge University Press).
[26] Gelbart, W. M., and Barboy, B., 1980, *Accts Chem. Res.* **13,** 290. Gelbart, W. M., 1982, *J. phys. Chem.*, **86,** 4296. (b) Mulder, B. and Ruijgrok, Th. W., 1982, *Physica* A, **113,** 145.
[27] Mezei, M., 1981, *J. comput. Phys.*, **39,** 128.
[28] Knuth, D. E., 1981, *The Art of Computer Programming*, Vol. 2 (Addison–Wesley).
[29] Control Data Corporation, 1979, Publ. No. 60483100 (CDC, Sunnyvale).
[30] Kalle, C., and Wansleben, S., 1984, *Comput. Phys. Commun.*, **33,** 343.
[31] Abramowitz, M., and Segun, I. A. (editors), 1964, *Handbook of Mathematical Functions* (Dover).
[32] IMSL, 1982, *Library Reference Manual*, 9th edition (IMSL).
[33] Landau, D. P., 1976, *Phys. Rev.* A, **13,** 2997; 1976, *Ibid.*, **14,** 255.
[34] Viellard-Barron, J., 1974, *Molec. Phys.*, **28,** 809.
[35] Zannoni, C., 1981, *Molec. Phys.*, **42,** 1303.
[36] Eppenga, R., and Frenkel, D., 1984, *Molec. Phys.*, **52,** 1303.
[37] Pershan, P. S., *The Molecular Physics of Liquid Crystals*, edited by G. R. Luckhurst and G. W. Gray (Academic Press), Chap. 17.
[38] Levine, R. D., and Tribus, M., 1978, *The Maximum Entropy Formalim* (MIT Press).
[39] Erdelyi, A, 1956, *Asymptotic Expansions* (Dover).
[40] Ryumtsev, E. I., and Tsvetkov, V. N., 1968, *Optics Spectrosc.*, **24,** 332.
[41] Gierke, T. D., and Flygare, W. H., 1974, *J. chem. Phys.*, **61,** 2231.
[42] Attard, G. S., Beckmann, P. A., Emsley, J. W., Luckhurst, G. R., and Turner, D. L., 1982, *Molec. Phys.*, **45,** 1125.